Supplementary Information

Supplementary Figures

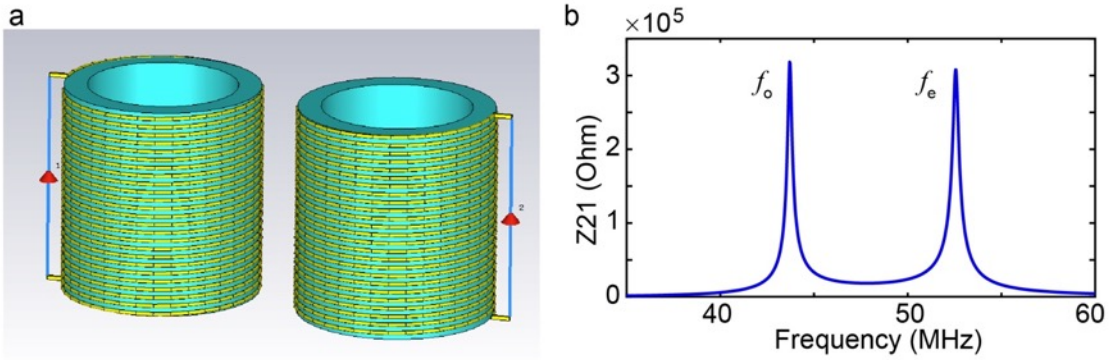

Supplementary Figure 1: Coupling coefficient numerical derivation. (a) Unit cell model employed in CST for coupling coefficient simulation. (b) The Z_{21} of the two ports with spacing of 38 mm between two unit cells demonstrating the resonant frequency splitting.

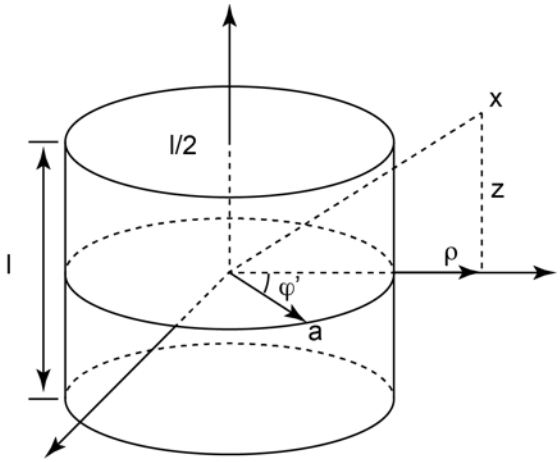

Supplementary Figure 2: Schematic drawing of the helix labeled with parameters used in Eq. S6 to S11 to derive the magnetic field strength.

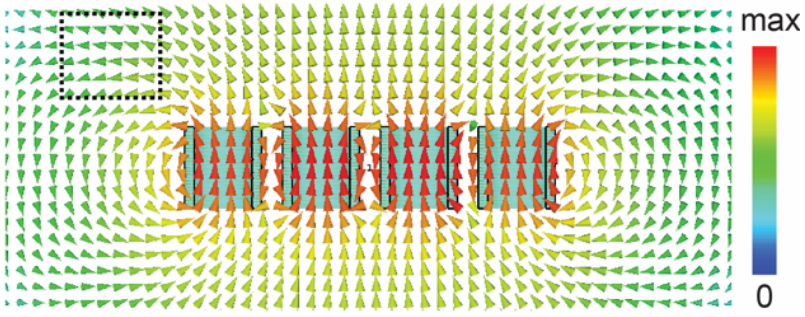

Supplementary Figure 3: Magnetic field vector distribution of the magnetic metamaterial at the resonance frequency.

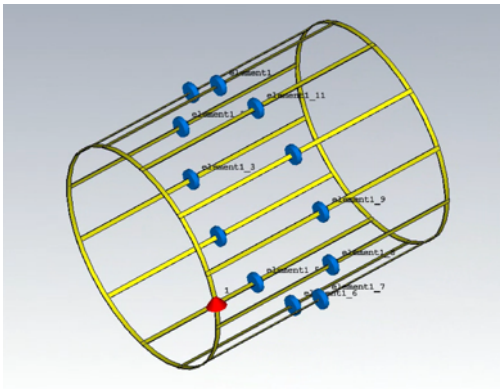

Supplementary Figure 4: Birdcage RF antenna employed during the simulations to derive the noise.

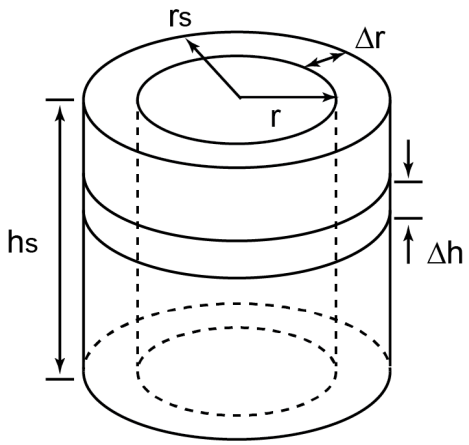

Supplementary Figure 5: Cylindrical sample with labeled geometry used in Eq. S15 to S19 to calculate the equivalent resistance.

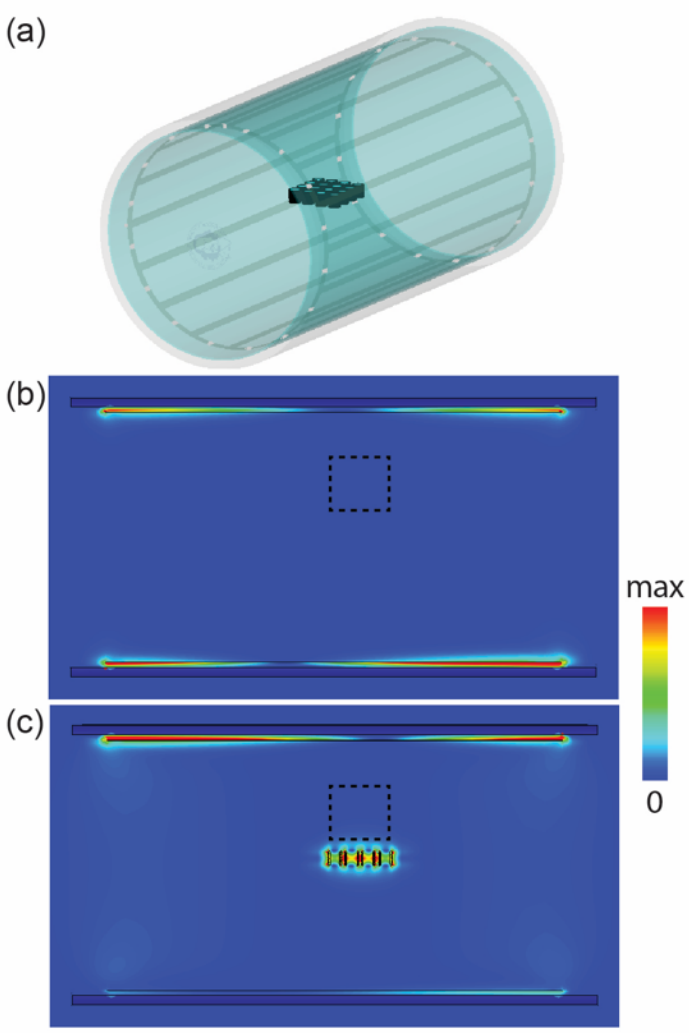

Supplementary Figure 6: Simulation of the electric field distribution in the MRI body coil. (a) The configuration for modeling the electric field. (b) and (c) are the simulation results of the electric field distribution with and without the MRI metamaterial, respectively. The dashed square indicates the location of the phantom.

Supplementary Tables

Supplementary Table 1. Parameters used in resistance derivation in Eqs. S13 and S14.

ω (rad)	$63.8\times10^{-7}\times2\pi$	r(mm)	15	ε_r	2
ρ(Ωm)	1.78×10^{-8}	a(mm)	0.28	C(F)	8.57×10^{-13}
μ_0(H/m)	$4\pi\times10^{-7}$	l(mm)	32		
n	25	ε_i	0.06		

Supplementary Notes

Supplementary Note 1: Coupling coefficient derivation based on simulation

In order to validate the coupling coefficient theoretical results, a numerical method was introduced to derive the coupling coefficient. Two adjacent helices were modeled using commercial electromagnetic field simulation software (CST Studio Suite 2017). The adjacent helices were modeled in CST as shown in Supplementary Figure 1a, in which two discrete ports were placed across the two helices. The simulated Z_{21} is depicted in Supplementary Figure 1b. The two peaks of Z_{21} indicate the two resonant modes of the coupled helices, and the splitting of the two peaks may be utilized to retrieve the coupling coefficient *(36)*:

$$k = \frac{f_o^2 - f_e^2}{f_o^2 + f_e^2} \tag{S1}$$

in which f_o (f_e) represents the resonant frequency of the mode with opposite (identical) current direction in the two unit cells. The simulated coupling coefficients as a function of unit cell separation distance are plotted in Fig. 2, demonstrating a high degree of agreement with the theoretical results.

Supplementary Note 2: Coupling mode theory derivation of resonant frequency and strength of each unit cell

The resonant mode and the resonant strength of each unit cell may be derived by utilizing the coupled mode theory, as shown in Eq. 4. By neglecting the loss (Γ_n), the resonant frequency and the corresponding resonant strength of each unit cell can be derived by solving the following equation matrix.

$$\frac{\mathrm{d}a_n(t)}{\mathrm{d}t} = -\mathrm{j}\omega_0 a_n(t) + \mathrm{j}\sum_{k=1}^{m,k\neq n} K_{kn} a_k(t),\ n = 1, \cdots, m \tag{S2}$$

For a 2 × 2 array with separation distance of 8 mm, the eigenvalue of the resultant matrix is:

$$A = \left[-59.82 \quad -49.84 \quad -49.84 \quad -43.20\right] \times 10^6$$

Each value corresponds to the frequency of a specific resonant mode. The eigenvector of the resultant matrix is:

$$V = \begin{bmatrix} 0.50 & -0.60 & -0.38 & 0.5 \\ 0.50 & -0.38 & 0.60 & -0.5 \\ 0.50 & 0.38 & -0.60 & -0.5 \\ 0.50 & 0.60 & 0.38 & 0.5 \end{bmatrix}$$

Each column corresponds to the resonant strength of each unit cell at a specific resonant mode with the resonant frequency in the exact column in A. The minus sign refers to the fact that the current is in the opposite direction. It can be seen that the current direction in each unit cell is identical for the resonant mode with the highest resonant frequency, which is employed for the magnetic field enhancement. By increasing the number of unit cells, the resonant frequency and the corresponding resonant strength may be readily calculated for larger arrays.

Supplementary Note 3: Magnetic field distribution and field enhancement

The induced voltage along the helix of the unit cell may be calculated as follows:

$$V = n\pi r^2 \frac{\mathrm{d}B_1}{\mathrm{d}t} \tag{S3}$$

where B_1 is the magnetic field strength of the MRI, n is the number of turns, and r is the radius of the helix. Furthermore, the impedance of the helix may be calculated as follows:

$$Z = \mathrm{j}\omega L + \frac{1}{\mathrm{j}\omega C} + R_{\mathrm{ohm}} + R_{\mathrm{dielec}} \tag{S4}$$

$$I = \frac{V}{Z} \tag{S5}$$

where L and C represent the equivalent inductance and capacitance of the helix (including the self-reactance and mutual reactance), respectively. The typical bandwidth of the MRI is 50 kHz, therefore, the working frequency was selected to be 300 kHz lower than the resonant frequency. We also note that when the frequency of the working mode is lower than the working frequency of MRI, the induced magnetic field will cancel the original magnetic field, resulting in even weaker field strength. Therefore, the frequency of the working mode was set to 300 kHz higher than the working frequency of the MRI, considering the bandwidth of the MRI (typically 50 kHz) for frequency encoding. The current can be evaluated with Eq. S5 by dividing Eq. S3 with Eq. S4.

At the resonant state, the current inside the helix exhibits a sinusoidal distribution with a maximum value at the middle and a value of zero at the two ends. The mean spatial current value can be calculated with Eq. S5 and with the maximum value $2^{-1/2}$-fold of the mean value. To simplify the calculation process, the helix can be assumed to be a continuous current sheet with the current density dependent on the amplitude of current in the middle of the helix (I_0), the number of turns (n), and the height of the helix (l). Assuming the helix along the z-axis is from $-l/2$ to $l/2$, as shown in Supplementary Figure 2, the current at the position of z' may be expressed as:

$$I_{\mathrm{d}} = \cos\left(\frac{\pi z'}{l}\right)\frac{I_0 n}{l} \tag{S6}$$

According to the Biot-Savart law, the magnetic field at any point in space can be expressed as:

$$B(x) = \frac{\mu_0 n I_0}{4\pi l}\int_{-l/2}^{l/2}\cos\left(\frac{\pi z'}{l}\right)\mathrm{d}z\int\frac{\mathrm{d}x'\times\vec{R}}{\left|\vec{R}\right|^3} \tag{S7}$$

in which $\vec{R}$ is the distance between the target point and the integral elements in the vector. Expanding the equation in polar coordinates:

$$\mathrm{d}x'\times\vec{R} = a\mathrm{d}\varphi'\left[\left(z-z'\right)\cos\varphi'\vec{\mathrm{i}}+\left(z-z'\right)\sin\varphi'\vec{\mathrm{j}}+\left(a-\rho\cos\varphi'\right)\vec{\mathrm{k}}\right] \tag{S8}$$

$$\left|\vec{R}\right| = \sqrt{\rho^2 - 2a\rho\cos\varphi' + a^2 + \left(z-z'\right)^2} \tag{S9}$$

in which ρ, φ, and z are the points in free space in polar coordinates, and a is the radius of the helix. Therefore, the magnetic field components along the axial and radial directions may be expressed:

$$B(z)=\frac{\mu_0 nI_0}{4\pi l}\int_{-l/2}^{l/2}\cos\left(\frac{\pi z'}{l}\right)\int_0^{2\pi}\frac{\left(a-\rho\cos\varphi'\right)}{\left[\rho^2-2a\rho\cos\varphi'+a^2+\left(z-z'\right)^2\right]^{3/2}}\mathrm{d}\varphi'\mathrm{d}z' \quad \text{(S10)}$$

$$B(\rho)=\frac{\mu_0 nI_0}{4\pi l}\int_{-l/2}^{l/2}\cos\left(\frac{\pi z'}{l}\right)\int_0^{2\pi}\frac{\left(z-z'\right)\cos\varphi'}{\left[\rho^2-2a\rho\cos\varphi'+a^2+\left(z-z'\right)^2\right]^{3/2}}\mathrm{d}\varphi'\mathrm{d}z' \quad \text{(S11)}$$

The magnetic field enhancement in an arbitrary coordinate system may be calculated by multiplying Eq. S10 with the relative resonant strength of each unit cell, adding the results for all the unit cells with the exciting magnetic field (B_1), and normalizing the summation by the exciting magnetic field. The calculation results are plotted in Fig. 4.

The direction of the magnetic field also varies at locations in the vicinity of the metamaterial. The simulation results, as shown in Supplementary Figure 3, demonstrate that the electric field is along the axial direction in the center of the metamaterial, but becomes tangential near the corners of the metamaterial. The variation in magnetic field direction, along with the magnetic field strength decay, ultimately determines the gradient of the SNR enhancement.

Supplementary Note 4: Resistance derivation in metamaterial unit cells

The resistance of the unit cells includes both the ohmic loss from the copper wire as well as the dielectric loss from the scaffolding core. Considering the skin depth of the wire, the ohmic loss may be calculated as follows:

$$R_{\mathrm{ohm}}=\sqrt{\frac{\omega\mu_0\rho}{2}}\frac{l_{\mathrm{t}}}{\pi a} \quad \text{(S12)}$$

$$l_{\mathrm{t}}=\sqrt{\left(n2\pi r\right)^2+l^2} \quad \text{(S13)}$$

in which ω is the angular frequency, ρ is the resistivity, μ_0 is the permeability of free space, l_t is the length of the copper wire, a is the diameter of the copper wire, n is the number of turns, r is the radius of the helix, and l is the height of the helix. This results in an ohmic loss of 2.78 Ω from the copper wire in the unit cell.

The dielectric loss from the scaffolding core may be calculated as follows:

$$R_{\mathrm{dielec}}=\frac{2\varepsilon_{\mathrm{i}}}{\omega C\left(\varepsilon_{\mathrm{r}}+1\right)^2} \quad \text{(S14)}$$

where ε_i and ε_r represent the real and imaginary permittivity of the core material, and C is the equivalent capacitance of the helix. This results in a dielectric loss of 38.8 Ω from the scaffolding core in the unit cell. All the parameters employed in the derivation process are listed in Table S1.

Supplementary Note 5: Noise derivation

The birdcage coil located within the bore of the MRI was simulated using commercial electromagnetic field simulation software (CST Studio Suite 2017) with a diameter of 0.5 m and a length of 0.6 m (Supplementary Figure 4). The excitation source was set to 1 ampere of current in the port. The excited magnetic field strength at the center of the coil was simulated as 1.93 A/m.

By substituting $B_1 = 1.93\mu_0$ T into Eq. S5, the current amplitude in the unit cell can be calculated as 0.28 A. The power dissipation rate can be transferred to an equivalent resistance serial connected in the excitation port as 3.26 Ω ($0.28^2 \times 41.58$). Assuming the number of unit cells in the array is 16, the total resistance from the metamaterial array is 52.16 Ω.

The loss of the sample to be imaged also introduces additional noise. The geometry of the target sample is assumed to be a cylinder with height and radius of h_s and r_s, respectively. The integration unit may be chosen as a ring, as shown in Supplementary Figure 5. The resistance for the unit is:

$$\Delta R = \frac{\rho 2\pi r}{\Delta r \Delta h} \tag{S15}$$

in which ρ is resistivity of the sample. The induced voltage can be derived as:

$$V = \pi r^2 \frac{\mathrm{d}B(h)}{\mathrm{d}t} \tag{S16}$$

in which $B(h)$ is the magnetic field strength related to the distance from the metamaterial array. The power dissipation rate is:

$$\Delta P = \frac{V^2}{\Delta R} = \pi^2 r^4 \frac{B(h)^2 \omega^2}{2} \frac{\Delta r \Delta h}{\rho 2\pi r} = \frac{\pi r^3}{4\rho} B(h)^2 \omega^2 \Delta r \Delta h \tag{S17}$$

in which ω is the angular frequency. A factor of 2 is introduced to yield the average power dissipation rate. The total power dissipation rate is:

$$P = \int_0^{r_s} \Delta r \int_0^{h_s} \Delta h \frac{\pi r^3}{4\rho} B(h)^2 \omega^2 \tag{S18}$$

In the absence of the metamaterial array, $B(h)$ is a constant value of $1.93\mu_0$ T, and Eq. S18 can be further simplified as:

$$P = \frac{\pi r_s^4 h_s}{16\rho} (1.93\mu_0)^2 \omega^2 \tag{S19}$$

Assuming the resistivity of the target sample is 0.85 Ωm (*37*), the radius is 0.05 m, and the height is 0.1 m, the calculated power dissipation rate is 0.14 watt, which can be transferred to the equivalent resistance in the port as 0.28 Ω. In the presence of the metamaterials, taking the enhancement ratio into consideration, the calculated power dissipation is 2.24 watt, which can be transferred to the equivalent resistance in the port as 4.48 Ω. The total equivalent resistance values with and without the metamaterials are 106.64 and 50.28 Ω, respectively, and, according to Eq. 6, the noise is increased by the factor of 1.46.

Supplementary Note 6: Effect of metamaterial on the electric field in MRI

In order to investigate the effect of the metamaterial on the electric field distribution in MRI, we performed numerical simulation using CST Studio Suite 2017 by considering the birdcage body coil and the magnetic metamaterials, as shown in Supplementary Figure 6a. In the absence of the metamaterial, the electric field is uniform and weak throughout the bore of the MRI. When the metamaterial is in place, the resonance of the metamaterial generates oscillating currents in the unit cells, leading to the generation of an electric field confined within the metamaterial unit cells, as shown in Supplementary Figure 6b. The electric field in the phantom area in the presence of the metamaterial

approximates the condition in the absence of the metamaterial in this region. These results indicate that the metamaterial has little effect on the electric field in the region of interest.